Applied Surface Science 528 (2020) 146591

Contents lists available at ScienceDirect

Applied Surface Science

journal homepage: www.elsevier.com/locate/apsusc

Why are MoS_2 monolayers not a good catalyst for the oxygen evolution reaction?

Estefania German[a,b,*], Ralph Gebauer[c]

[a] Departamento de Física Teórica, Atómica y Óptica, Universidad de Valladolid, 47011 Valladolid, Spain
[b] Instituto de Física del Sur (IFISUR), Departamento de Física, Universidad Nacional del Sur (UNS), CONICET, Av. L. N. Alem 1253, B8000CPB Bahía Blanca, Argentina
[c] The Abdus Salam International Centre for Theoretical Physics (ICTP), Strada Costiera 11, 34151 Trieste, Italy

ARTICLE INFO

Keywords:
Oxygen evolution reaction
Water splitting
Transition metal dichalcogenide
MoS_2
Density functional theory

ABSTRACT

We use density functional theory based calculations to study the energetics of the oxygen evolution reaction on a monolayer of MoS_2. This material, a prototypical example of a layered transition metal dichalcogenide, is intensely studied in the context of many important catalytical applications, in particular for the hydrogen evolution reaction. The second half-reaction of the water-splitting process, the oxygen evolution reaction, is almost never considered on this material, due to its low activity. Based on our calculations, we explain this experimentally observed poor catalytic activity for the oxygen evolution by the weak binding of two key reaction intermediates (hydroxyl and hydroperoxyl) to the substrate. We explore substitutional doping with oxygen and phosphorous as means to facilitate the oxygen evolution on MoS_2 layers. The oxygen substitution slightly increases the reaction's overpotential, but does not significantly change the energetics. The doping with phosphorous, on the other hand, is not a promising way to promote the oxygen evolution on MoS_2 layers. We also explore the role of the edges of MoS_2 layers. We find that while the adsorption energies of reaction intermediates are strongly influenced by the presence of an edge, the final reaction overpotential remains nearly the same as on a pristine monolayer, meaning that the presence of edges is not favoring the OER.

1. Introduction

Using sustainable sources of energy like solar or wind to replace fossil fuels is the most important step in any effort to reduce the release of CO_2 into the atmosphere [1]. The intermittent nature of solar and wind power calls for an efficient way to store the energy. Storage in the form of chemical bonds is one possibility, for example by synthesis of liquid hydrocarbons from CO_2 and H_2 [2,3]. One key ingredient for such a scheme is an efficient way to split water into hydrogen and oxygen, either by electrolysis or directly using sunlight in a photo-electrochemical process. The "green" hydrogen which is thus produced from sustainable energy can either be stored or used subsequently as feedstock to produce hydrocarbons (in so-called power-to-liquids approaches [2]). Because of this central role which the hydrogen production holds in a renewable energy landscape, a lot of research has been devoted to the development of efficient catalysts for water splitting. Ideally, such a catalyst should consist of earth-abundant materials, be stable under working conditions, and require only a small overpotential for the desired reaction. Furthermore, it should exhibit large carrier mobilities and suitably aligned valence and conduction band edges with respect to the water oxidation and proton reduction levels, respectively.

The splitting of water,

$$2H_2O \rightarrow 2H_2 + O_2, \quad (1)$$

can be separated into two half-reactions, the hydrogen evolution reaction (HER),

$$2H^+ + 2e^- \rightarrow H_2, \quad (2)$$

and the oxygen evolution reaction (OER),

$$2H_2O \rightarrow 4H^+ + 4e^- + O_2. \quad (3)$$

In a water splitting device, these two half-reactions typically take place at the surface of two different materials which are connected electrically and by an electrolyte which serves as transport medium for the protons.

Four distinct proton-coupled electron transfer (PCET) steps are involved in the OER, while only two such steps are needed in the HER. For this reason, the OER is generally considered a much more difficult reaction to catalyze than the HER.

* Corresponding author.
E-mail address: estefania.german@uva.es (E. German).

https://doi.org/10.1016/j.apsusc.2020.146591
Received 2 March 2020; Received in revised form 23 April 2020; Accepted 2 May 2020
Available online 24 June 2020
0169-4332/

Many different kinds of materials have been investigated as potential catalysts for the electrochemical and photo-electrochemical splitting of water. While for the HER often platinum is used as electrode material, many different classes of materials have attracted interest as potential catalysts for the OER. Especially metal oxides have been used to oxidize water, like for example Fe_2O_3 or WO_3. The large band gap of many oxides minimizes in a photo-electrochemical setup the available portion of the solar spectrum. Also, poor carrier mobilities are reasons to look for alternatives to oxides. In this context, two-dimensional layers of transition-metal dichalcogenides (TMDs) [4,5] have recently stirred interest as potential catalysts. Especially the sulfides have as valence band maximum higher lying p-levels than the corresponding oxides, which leads to better suited band gaps and level alignments with respect to the water oxidation level. Furthermore, the two-dimensional nature of the TMD layers provides an easy path for carrier transport and leads to an increased specific surface area with respect to the bulk material.

MoS_2 is a typical example of a TMD which has shown promise in the context of many different catalytic reactions [6,7], ranging from CO_2 reduction [8–10] to CO hydrogenation [11] and the HER [12–16]. It is interesting to note that while many studies have concentrated on monolayer MoS_2 as catalyst for the HER, it is only rarely mentioned as a candidate for the OER. This is *a priori* surprising, as the valence band edge of monolayer MoS_2 is more positive than the oxidation potential of water (1.23 V vs. standard hydrogen electrode (SHE)), which should enable this material to promote the OER [17–19]. This general lack of experimental work on oxygen evolution on layers of MoS_2, an otherwise closely studied material [20–23], indicates that its potential is considered very limited for this particular reaction. And indeed, in a recent experimental study Pesci and coworkers have focused on layers of MoS_2 and WS_2 as OER catalysts [24], and found that while both materials can evolve O_2 gas in an acidic environment, the activity of MoS_2 is much weaker than that of WS_2, while the efficiency of MoS_2/WS_2 heterojunctions shows an increase by approximately one order of magnitude. The authors ascribe this improved efficiency of the heterojunction to an enhancement of electron-hole separation at the interface of the two materials. In this paper we investigate, by means of density-functional theory (DFT) based calculations, why monolayers of MoS_2 are not well suited to promote the OER in spite of a favorable band alignment.

The remainder of this paper is organized as follows. In Section 2 we describe the structure of MoS_2 monolayers and how we model them in a periodic density-functional theory setup. In Section 3 we give details about the theoretical approach, both for the electronic structure calculations (Section 3.1) and how we model the PCET process (Section 3.2). Our results are shown and discussed in Section 4.

2. Structure of MoS_2 layers

MoS_2 has, like most group 4–7 TMDs a graphite-like layered structure. Each layer consists of three sheets: one Mo sheet that is sandwiched between two S sheets. This triatom-layer has a thickness of 3.14 Å. Within the layer, the Mo and S atoms are bound covalently, forming a hexagonal layer with a trigonal prismatic (D_{3h}) structure [4], also known as 1T. In bulk MoS_2, the individual layers are bound by van der Waals (vdW) forces, which allows for a relatively easy cleaving of the material in individual monolayers. In Fig. 1(a) and (b) such a layer of MoS_2 is shown.

In order to model a single monolayer of MoS_2, we include 13 Å of vacuum between the periodically repeated layers. This amount of space has been tested to effectively decouple the periodic images. Within each layer, we use a 5×5 supercell, containing thus 25 formula units of MoS_2 for a total of 75 atoms. In Fig. 1(a) four such unit cells are shown, delimited by solid black lines.

The choice of a 5×5 supercell (with a side length of 15.84 Å) enables us to adsorb various reaction intermediates on the surface while reducing to a minimum the spurious lateral interactions between an adsorbate and its periodic images.

We also consider the edges of MoS_2 monolayers. An *infinite stripe model* [25–28] is used for the edge simulations. In practice, a 4×4 MoS_2 supercell is periodically repeated in one direction only, leading to a stripe which exposes two inequivalent edges, as shown in Fig. 1(c). The sulfur-edge exposes the outermost sulfur atoms of the hexagonal lattice. Like for the sulfur atoms inside the monolayer, there are two S-atoms stacked above and below the Mo-layer. Every S-atom is bonded to two of the outermost Mo atoms, each of which is in turn bound to four S atoms on the edge. The S-edge resembles therefore a simple cut of the MoS_2 layer, apart from a slight relaxation of the edge atoms which is due to the reduced coordination of the sulfur atoms. This edge structure is also depicted in Fig. 1(e).

The molybdenum edge in its lowest energy configuration is covered with half a monolayer of sulfur [26–28], i.e. also the Mo-edge in terminated by S. As shown in Fig. 1(c), each one of the outermost Mo atoms is bound to one single terminal S atom. Those edge-terminating atoms lie in the plane of the Mo atoms (see Fig. 1(d)). Interestingly, these outermost sulfur atoms bind pairwise to one S neighbour, with a long bonding distance of 2.19 Å. Therefore, the sheet's Mo-edges are covered by pairs of weakly bound S atoms. The distance between the non-bound sulfur atoms on the edge is 4.20 Å.

3. Methods

3.1. DFT calculations

All our calculations are performed in a plane-wave (PW) and pseudopotential (PP) framework, as implemented in the Quantum ESPRESSO suite of electronic-structure programs [29,30], in particular using the PWscf code in version 6.4. This program employs DFT to solve the electronic many-body problem, while the nuclei are treated classically. Inherently, this approach relies on periodic boundary conditions at the edges of the simulation cell. For this reason a slab geometry with vacuum and a supercell within the MoS_2 layer has been adopted, as explained in Section 2.

The electronic exchange and correlation functional is approximated using the generalized gradient approximation in the parametrization of Perdew, Burke, and Ernzerhof (PBE) [31]. Because of the importance of vdW forces in physisorbed systems and the known problems with such interactions in the standard semilocal DFT approximations, we also include a dispersion correction, known as Grimme-D3 [32].

The Kohn–Sham (KS) orbitals are represented using PWs up to a kinetic energy cutoff of 45 Ry, and the electronic density with PWs up to 360 Ry. The two-dimensional Brillouin zone (BZ) has been sampled with a single shifted k-point, leading to three nonequivalent by symmetry k-points in the full BZ. In the case of the one-dimensional stripe, the BZ has been sampled with a grid of four shifted k-points in the direction of the stripe. Convergence with respect to the cutoff energies and k-point sampling has been carefully checked. We use an unrestricted spin-polarized formalism throughout.

The occupations of the KS are fixed using an efficient smearing scheme due to Marzari and Vanderbilt [33], using a fictitious electronic temperature of 13.6 meV. This smearing is introduced here merely to facilitate the convergence of the self-consistent field scheme. In contrast to the infinite monolayer, the edge structures do not have an electronic band gap. Therefore we use a larger fictitious electronic temperature of 136 meV for the calculation of the infinite stripe, which is necessary to converge the electronic structure in these open-shell edge structures.

The electron–ion interactions are modeled using Vanderbilt's ultrasoft PPs [34]. The PPs have 14, 6, 6, 5, and 1 valence electrons for Mo, S, O, P and H, respectively. All PPs can be found in the Standard Solid-State Pseudopotentials (SSSP) database [35,36].

Minimum energy configurations of all structures are found using structural relaxations with a Broyden–Fletcher–Goldfarb–Shanno (BFGS) algorithm. The geometries were relaxed until the residual forces

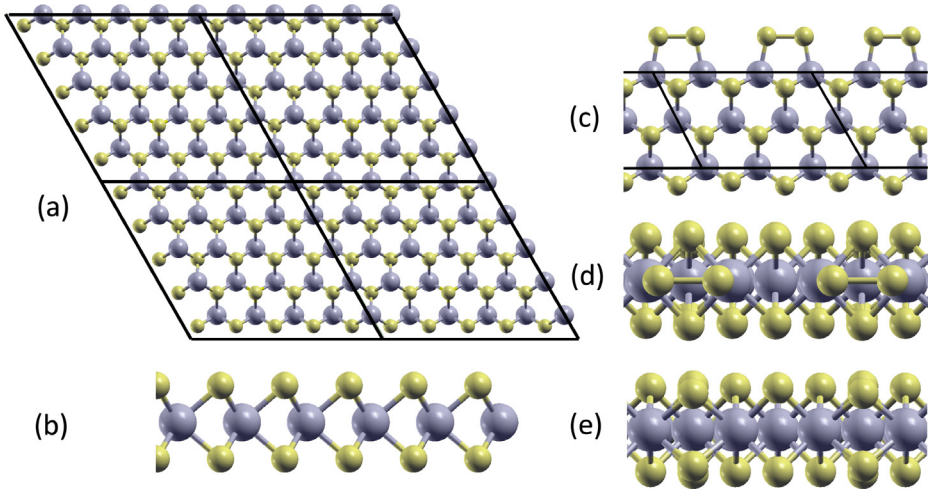

Fig. 1. Structure of a MoS_2 monolayer and its edges. (a) Top view of the infinite monolayer, the black lines indicate the size of the computational supercell used. (b) Side view of the infinite layer. (c) Infinite stripe model for the edge structures. The black lines indicate the 4 × 4 cell which is repeated periodically in the direction of the stripe. The top edge is the Mo-edge, covered by half a monolayer of S (see text). The bottom edge is the S-edge. (d) Side view of the Mo edge. (e) Side view of the S edge.

on all atoms were below a threshold of 25 meV/Å.

3.2. Proton-coupled electron transfer

The evolution of one O_2 molecule from two water molecules requires four distinct PCET steps. In each step different reaction intermediates are involved. Those intermediates are adsorbed to the catalyst. Since the over-all water splitting reaction is energetically an uphill process, an external source needs to provide energy for the splitting to proceed. This energy transfer needs to be such that each one of the four PCET steps is energetically favorable. In practice, this energy is provided either by an electric potential on the electrode (in electrolysis) or from excited electrons or holes in the case of photo-electrochemical water splitting. The same external energy is provided by each one of the four electrons (or holes) involved, while the four different intermediates will generally bind with different strength to the catalyst. These different binding energies lead to different external energy requirements for each one of the four PCET processes. It is the energetically highest one of the four steps which determines the required external energy. Thermodynamically, the evolution of one O_2 molecule requires an energy of 4.92 eV. For this reason, an ideal catalyst should lead to reaction steps of 1.23 eV for each one of the four PCETs. In this case, all the externally provided energy could be used for the desired reaction. The difficulty in finding a good OER catalyst comes from the fact that four different reaction intermediates will need to have suitable binding energies on its surface, and the steps should be as close to 1.23 eV as possible. The difference between the largest energy step and the ideal step leads to the so-called overpotential which is the energy lost in the form of heat during the other three steps.

The PCETs involved can generally be written as

$$(AH)^* \rightarrow (A)^* + H^+ + e^-, \quad (4)$$

where A and AH are reaction intermediates, the ∗ indicates binding to the catalyst, and on the right hand side the proton is in solution and the electron moved to the electrode. In order to estimate the energy step of this reaction, it is necessary to know the energy of a proton in solution and of an electron. Since these two quantities are difficult to extract from a simulation [37], we employ the method of the "computational hydrogen electrode" (CHE) pioneered by Nørskow and collaborators [38]. In this approach, the two energies are not determined separately, but one makes use of the fact that under standard conditions the free energy of $(H^+ + e^-)$ is equal to the free energy of 1/2 H_2. This fact allows one to obtain the energy required for a general PCET reaction like (4). It is important to note that the CHE approach only provides energy differences between the various reaction intermediates (which we call "step heights" here). It does not provide the reaction paths and therefore the barriers for each one of the steps. This is because the gradual solvation of desorbed protons is not explicitly simulated, and neither is the charging with an electon. For an approach to simulate such processes explicitly, we refer the reader to Ref. [37].

The four PCET steps involved in the OER are schematically represented in Fig. 2 as steps A to D. A water molecule adsorbs to the MoS_2 layer and loses one proton and one electron in step A, leading to a surface hydroxyl group. That group is further deprotonated and loses a second electron in step B. The second water molecule adsorbs and one further PCET happens in step C, leading to a surface bound hydroperoxy group. The final step D sees the desorption of an oxygen molecule and the final PCET, leading thus back to the starting configuration of the cycle.

4. Results and discussion

DFT calculations with structural relaxations as described in Section 3.1 have been performed for the bare MoS_2 layer as well as for the layer with the three reaction intermediates HO∗, O∗, and HOO∗. All the

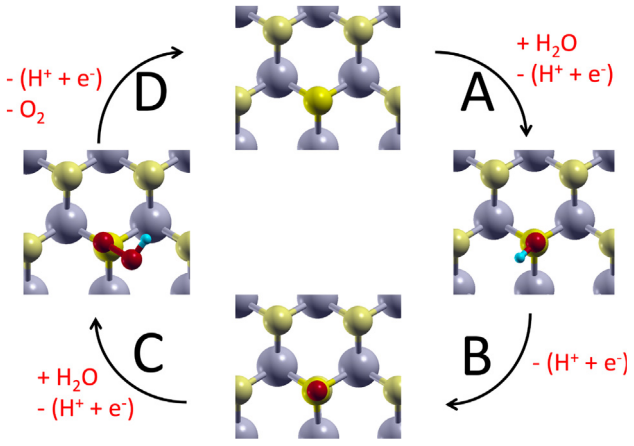

Fig. 2. Schematical representation of the four PCET steps and the reaction intermediates of the OER. Grey, yellow, red and blue balls represent Mo, S, O, and H atoms, respectively. (For interpretation of the references to colour in this figure legend, the reader is referred to the web version of this article.)

Table 1
Adsorption geometries on a MoS_2 monolayer. All distances in Å.

System	Intermediate				
		d(S–O)	d(O–H)	d(S–O(H))	
	O∗HO∗	1.510	1.012	1.702	
Undoped	HO∗	–	0.980	1.854	
	O∗	1.488	–	–	
		d(P–O(H))	d(O—H)	d(S—O)	d(P—O)
	O∗HO∗	1.611	1.003	1.510	–
P-doped	HO∗	1.628	0.977	–	–
	O∗	–	–	–	1.502
		d(S–O)	d(O–H)	d(S–O(H))	d(O–O)
	O∗HO∗	1.494	0.981	1.803	–
O-doped	HO∗	–	0.981	–	2.332
	O∗	1.488	–	–	–

intermediates are found to bind stably to the catalyst, with geometries as given in Table 1. The adsorption geometries are also depicted in Fig. 3. All intermediates bind to sulfur atoms, the binding to Mo is energetically not favorable or even impossible in all cases considered. Note that the most stable binding of the hydroperoxy group is dissociative, where one oxygen and one hydroxyl group bind to neighbouring sulfur atoms (see panel (c) in Fig. 3). We call this configuration O∗HO∗ in the following.

In Fig. 4 we show the corresponding energy diagram for the four PCET steps discussed above. Let us first concentrate on the perfect MoS_2 monolayer, shown as the black line in Fig. 4. It is immediately clear that this diagram is far from an ideal "staircase" scenario where each subsequent PCET step corresponds to an increase in energy of 1.23 eV. Indeed, the highest step is A, amounting to 2.36 eV. In this scenario, we obtain a prohibitively large overpotential of 1.13 V for the OER to proceed. This high step is a consequence of the relatively high energy of the HO∗ configuration with respect to what would be ideal for an OER catalyst. The negative step height for reaction B is a sign of the same fact: The energy level of the O∗ intermediate would be close to ideal, because with 1.90 eV it is not far from the ideal value of 2.46 eV. However, the high energy of the HO∗ intermediate leads to a negative step height for B.

The second highest step in this cycle is C, which amounts to 2.18 eV. Also here, the reason for this high step is the relatively weak binding of the O∗HO∗ reaction intermediate.

From the above considerations we can answer the question raised in the title of this publication: the ideal MoS_2 monolayer is a poor catalyst

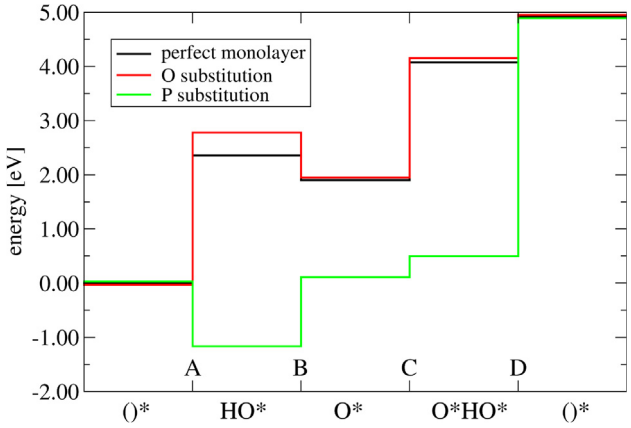

Fig. 4. Energy diagram for the four PCET steps of the OER on a monolayer of MoS_2.

for the OER reaction because two intermediates, HO∗ and O∗HO∗, while stable on the monolayer, have a weak binding energy, leading thus to huge overpotential for the water splitting.

This finding points into the direction of how one might potentially improve the catalytic activity of this material: if the binding of the two intermediates can be strengthened while leaving the binding energy of the O∗ intermediate unchanged, the overpotential would be reduced. We have investigated two possibilities for such an improvement: a substitutional doping with either O or P in the place of sulfur.

The case of the iso-electronic oxygen substitution is shown in Fig. 4 as a red line. It is immediately clear that, while not changing drastically the picture with respect to the perfect monolayer, the change is not favorable: step A is even higher in this case, amounting to 2.78 eV, an overpotential of 1.55 V.

The situation is much more drastic when the valency of the substitutional atom is changed. The case of P doping is shown as a green line in Fig. 4. Here, the binding of the HO∗ intermediate is much stronger, leading to a negative step height for process A. The exceedingly strong binding on the P doped monolayer which affects consequently all three intermediates manifests itself in the 4.42 eV high step D. Indeed, in the case it is the empty P-doped layer which has a very high energy (and reactivity) due to the dangling bond present there.

It is not realistic to assume that a P-doped monolayer in contact with the electrolyte would remain pristine. Instead, it would be energetically

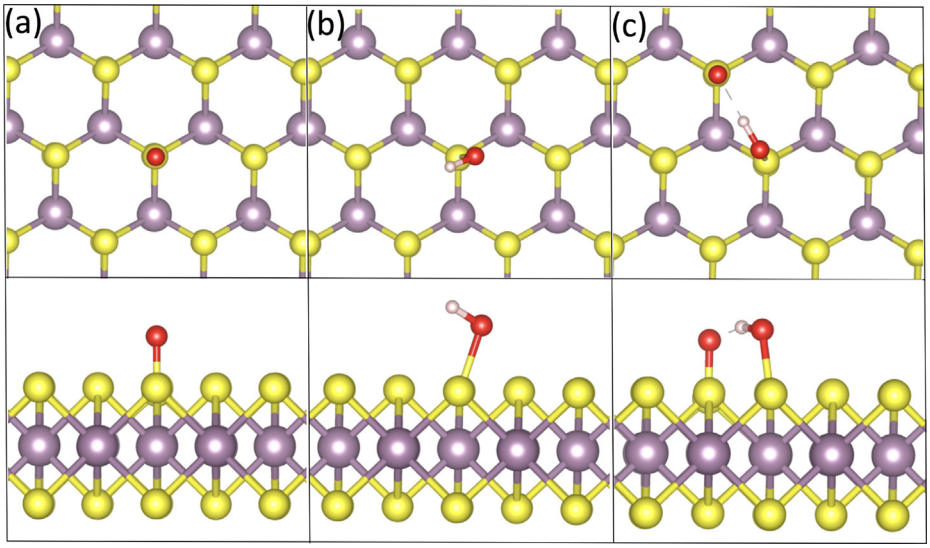

Fig. 3. Adsorption geometries of reaction intermediates for the OER cycle on a pristine MoS_2 layer. (a) The O∗ intermediate, (b) the HO∗ intermediate and (c) the O∗HO∗ intermediate.

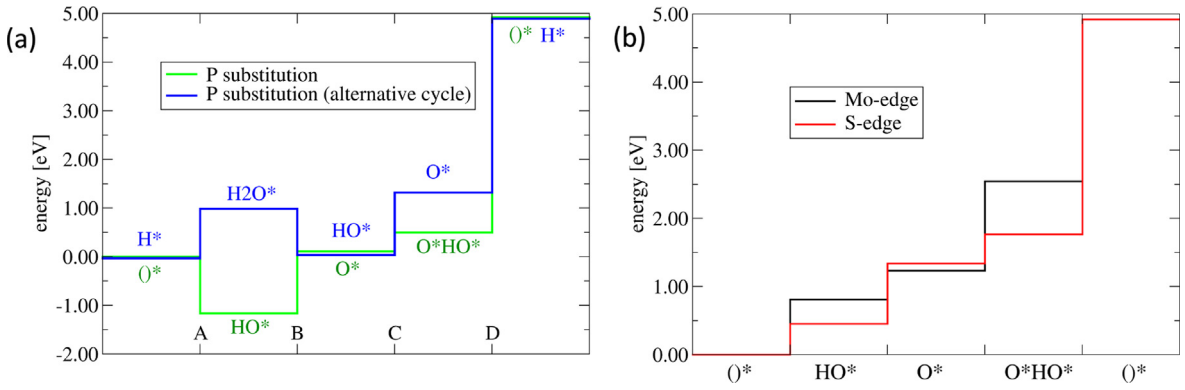

Fig. 5. Energy diagram for the four PCET steps of the OER. (a) On a monolayer of MoS_2 with substitutional P doping. Two distinct PCET cycles are considered (see text). (b) At the two edges of a MoS_2 stripe.

favorable for the system to saturate the dangling bond with a proton from the electrolyte, leading to a partially protonated state. We have also considered this possibility, where the OER cycle would be slightly different than shown in Fig. 2. Starting from a protonated active site, steps A and B remain the same as in the original cycle: adsorption of a water molecule together with a deprotonation, followed by the second deprotonation in step B. In the alternative cycle, step C is the third deprotonation, leading to an O∗ reaction intermediate. In the final step D the second water molecule is adsorbed, together with the final deprotonation and the release of an oxygen molecule. The energy levels corresponding to this alternative cycle are depicted in Fig. 5(a) where also the new reaction intermediates are indicated (blue lines and labels). While this more realistic cycle for the P doped monolayer indeed shows a somewhat smaller height for step D, it is with 3.60 eV still to high for any conceivable application.

Given that the surface of the monolayer is not favorable for catalyzing the OER, we have also examined the two most stable edge configurations of this material. On the Mo-edge, covered by half a monolayer of S, all reaction intermediates bind to the edge sulfur atoms. When this happens, the weak dimer binding between two adjacent S atoms is broken and the distance between the previously paired sulfur atoms increases. The neighbouring sulfur dimers on the edge are not dissociated in this process. The structures of the bound reaction intermediates are depicted in Fig. 6(a)–(c), and the corresponding geometries are given in Table 2. As it is the case for the binding on the surface of the monolayer, also in this edge configuration the OOH reaction intermediate binds dissociatively as O∗HO∗, see Fig. 6(c).

A similar picture emerges for the binding on the S-edge. Also here, the OOH reaction intermediate dissociates and binds as O∗HO∗, see Fig. 6(f). Both the oxygen atom of this configuration and the O reaction intermediate, see Fig. 6(d), bind in a bridging position between one of the edge-S and one of the outermost Mo atoms. The HO∗ reaction intermediate directly binds on-top of an edge-S atom.

Table 2
Adsorption geometries at the edges of a MoS_2 monolayer. All distances in Å.

System	Intermediate				
		d(S–O(H))	d(O–H)	d(S–O)	
	O∗HO∗	1.704	0.979	1.481	–
Mo-edge	HO∗	1.702	0.980	–	–
	O∗	–	–	1.480	–
		d(S–O(H))	d(O–H)	d(S–O)	d(Mo–O)
	O∗HO∗	1.661	0.985	1.606	2.171
S-edge	HO∗	1.664	0.986	–	–
	O∗	–	–	1.605	2.168

The energetics of the OER cycle in these two edge-configurations is shown in Fig. 5(b). In contrast to what happens on the surface of the monolayer, the edge configurations both lead to a staircase-like energetic order for the four PCET steps. This is desirable, but the highest step still amounts to 2.38 eV (3.15 eV) on the Mo-edge (S-edge). This corresponds to an overpotential of 1.15 V and 1.92 V, respectively. The lower one of these overpotentials is nearly the same as on the pristine monolayer, where we have found it to be 1.13 V (see above).

These findings show that the presence of edge sites of MoS_2 layers does not improve the catalytic behaviour of this material for the OER.

5. Conclusions

We have employed DFT based calculations to investigate the OER on a monolayer of MoS_2. This material is actively investigated for various catalytic applications, and has also shown to be able to evolve O_2 [24], albeit with a very low activity. The alignment of the material's energy levels with respect to the relevant redox levels of the electrolyte is favorable, so the question arises about the reasons for this low activity.

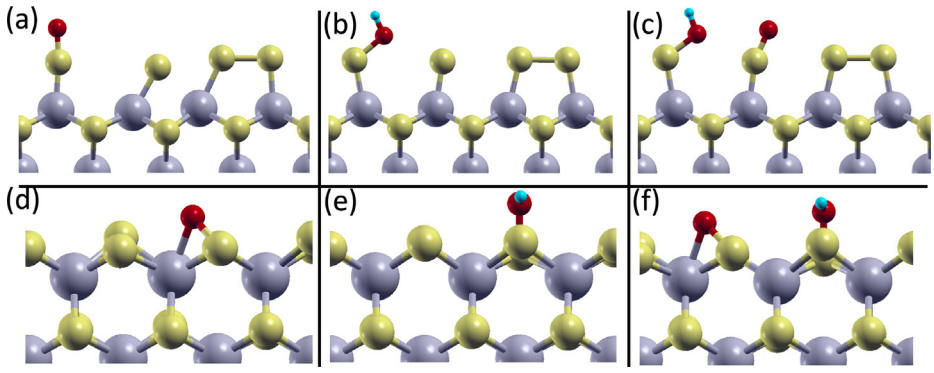

Fig. 6. Adsorption geometries on the edges of the MoS_2 layer. (a)–(c) Mo-edge (d)—(f) S-edge.

Here we show that the low catalytic activity is due to the weak binding of the HO* and HOO* reaction intermediates with respect to the O* intermediate, which leads to a high overpotential of 1.13 V. This overpotential is the reason for the observed trends.

We have investigated substitutional doping with oxygen or phosphorous as possible ways to alter the binding energies and thus to potentially reduce the overpotential for the OER. While such substitutions indeed alter the rate determining steps in the catalytic cycles, none of them is able to lead to a more favorable situation for the OER. Similarly, we have examined the situation at the edges of MoS_2 layers. The two most common edges, namely the sulfur-edge and the molybdenum edge, covered by half a monolayer of S, have been considered. The coordination of Mo and S atoms at the edges varies with respect to the pristine layer. Consequently we find that the adsorption energies of the four PCET reaction intermediates are altered. However, these different adsorption energies do not lead to a more favorable situation for the OER: the overpotential is found to be 1.15 V at the Mo-edge, a value nearly identical to the overpotential on the pristine MoS_2 monolayer. On the S-edge, the overpotential is considerably higher (1.92 V) which makes that edge configuration even less favorable for the OER.

Future investigations of this class of materials will focus on heterojunctions of MoS_2 with different TMDs which, as has recently been shown experimentally [24] can lead to promising results for the evolution of oxygen in a photo-electrochemical context.

Compliance with ethical standards

The authors declare that they have no conflict of interest.

CRediT authorship contribution statement

Estefania German: Conceptualization, Methodology, Validation, Formal analysis, Investigation, Writing - original draft, Writing - review & editing. **Ralph Gebauer:** Conceptualization, Methodology, Validation, Formal analysis, Investigation, Writing - original draft, Writing - review & editing.

Declaration of Competing Interest

The authors declare that they have no known competing financial interests or personal relationships that could have appeared to influence the work reported in this paper.

Acknowledgements

E.G. would like to thank the ICTP and the Simons Foundation for providing the opportunity to undertake this research by supporting her visit to the ICTP as an ICTP-Simons Associate.

References

[1] Richard J. Millar, Jan S. Fuglestvedt, Pierre Friedlingstein, Joeri Rogelj, Michael J. Grubb, H. Damon Matthews, Ragnhild B. Skeie, Piers M. Forster, David J. Frame, Myles R. Allen, Emission budgets and pathways consistent with limiting warming to 1.5 C, Nat. Geosci. 10(10) (2017) 741–747.
[2] Jan Christian Koj, Christina Wulf, Petra Zapp, Environmental impacts of power-to-X systems – a review of technological and methodological choices in Life Cycle Assessments, Renew. Sustain. Energy Rev. 112 (2019) 865–879.
[3] Zhifei Yan, Jeremy L. Hitt, John A. Turner, Thomas E. Mallouk, Renewable electricity storage using electrolysis, Proc. Natl. Acad. Sci. (2019) 201821686.
[4] Manish Chhowalla, Hyeon Suk Shin, Goki Eda, Lain-Jong Li, Kian Ping Loh, Hua Zhang., The chemistry of two-dimensional layered transition metal dichalcogenide nanosheets, Nat. Chem. 5(4) (2013) 263–275.
[5] Changrong (Rose) Zhu, Daqiang Gao, Jun Ding, Dongliang Chao, John Wang, TMD-based highly efficient electrocatalysts developed by combined computational and experimental approaches, Chem. Soc. Rev. 47(12) (2018) 4332–4356.
[6] P. Raybaud, J. Hafner, G. Kresse, S. Kasztelan, H. Toulhoat, Structure, energetics, and electronic properties of the surface of a promoted MoS2 catalyst: an ab initio local density functional study, J. Catal. 190 (1) (2000) 128–143.
[7] Oleg V. Yazyev, Andras Kis, MoS 2 and semiconductors in the flatland, Mater. Today 18 (1) (2015) 20–30.
[8] Mohammad Asadi, Mohammad Hossein Motevaselian, Alireza Moradzadeh, Leily Majidi, Mohammadreza Esmaeilirad, Tao Victor Sun, Cong Liu, Rumki Bose, Pedram Abbasi, Peter Zapol, Amid P. Khodadoust, Larry A. Curtiss, Narayana R. Aluru, Amin Salehi-Khojin, Highly efficient solar-driven carbon dioxide reduction on molybdenum disulfide catalyst using choline chloride-based electrolyte, Adv. Energy Mater. 9(9) (2019) 1803536.
[9] Qiao Sun, Gangqiang Qin, Yingying Ma, Weihua Wang, Ping Li, Du. Aijun, Zhen Li, Electric field controlled CO2 capture and CO2/N 2 separation on MoS2 monolayers, Nanoscale 9 (1) (2017) 19–24.
[10] Duy Le, Takat B. Rawal, Talat S. Rahman, Single-layer MoS2 with sulfur vacancies: structure and catalytic application, J. Phys. Chem. C 118 (10) (2014) 5346–5351.
[11] Min Huang, Kyeongjae Cho, Density functional theory study of CO hydrogenation on a MoS 2 surface, J. Phys. Chem. C 113 (13) (2009) 5238–5243.
[12] Yanguang Li, Hailiang Wang, Liming Xie, Yongye Liang, Guosong Hong, Hongjie Dai, MoS 2 nanoparticles grown on graphene: an advanced catalyst for the hydrogen evolution reaction, J. Am. Chem. Soc. 133 (19) (2011) 7296–7299.
[13] Mark A. Lukowski, Andrew S. Daniel, Fei Meng, Audrey Forticaux, Linsen Li, Song Jin, Enhanced hydrogen evolution catalysis from chemically exfoliated metallic MoS 2 nanosheets, J. Am. Chem. Soc. 135 (28) (2013) 10274–10277.
[14] Damien Voiry, Maryam Salehi, Rafael Silva, Takeshi Fujita, Mingwei Chen, Tewodros Asefa, Vivek B. Shenoy, Goki Eda, Manish Chhowalla, Conducting MoS 2 nanosheets as catalysts for hydrogen evolution reaction, Nano Lett. 13 (12) (2013) 6222–6227.
[15] Yu. Yifei, Sheng-Yang Huang, Yanpeng Li, Stephan N. Steinmann, Weitao Yang, Linyou Cao, Layer-dependent electrocatalysis of MoS 2 for hydrogen evolution, Nano Lett. 14 (2) (2014) 553–558.
[16] Jing Zhang, Wu Jingjie, Hu.a. Guo, Weibing Chen, Jiangtan Yuan, Ulises Martinez, Gautam Gupta, Aditya Mohite, Pulickel M. Ajayan, Jun Lou, Unveiling active sites for the hydrogen evolution reaction on monolayer MoS 2, Adv. Mater. 29 (42) (2017) 1701955.
[17] Jun Kang, Sefaattin Tongay, Jian Zhou, Jingbo Li, Wu. Junqiao, Band offsets and heterostructures of two-dimensional semiconductors, Appl. Phys. Lett. 102 (1) (2013) 012111.
[18] Arunima K. Singh, Kiran Mathew, Houlong L. Zhuang, Richard G. Hennig, Computational screening of 2D materials for photocatalysis, J. Phys. Chem. Lett. 6 (6) (2015) 1087–1098.
[19] Bishnupad Mohanty, Mahdi Ghorbani-Asl, Silvan Kretschmer, Arnab Ghosh, Puspendu Guha, Subhendu K. Panda, Bijayalaxmi Jena, Arkady V. Krasheninnikov, Bikash Kumar Jena, MoS 2 quantum dots as efficient catalyst materials for the oxygen evolution reaction, ACS Catal. 8 (3) (2018) 1683–1689.
[20] Xiao Li, Hongwei Zhu, Two-dimensional MoS2: properties, preparation, and applications, J. Mater. 1 (1) (2015) 33–44.
[21] Hongxing Li, Min Huang, Gengyu Cao, Markedly different adsorption behaviors of gas molecules on defective monolayer MoS 2: a first-principles study, Phys. Chem. Chem. Phys. 18 (22) (2016) 15110–15117.
[22] Jia Zhu, Hui Zhang, Yawen Tong, Ling Zhao, Yongfan Zhang, Yuzhi Qiu, Xianning Lin, First-principles investigations of metal (V, Nb, Ta)-doped monolayer MoS2: Structural stability, electronic properties and adsorption of gas molecules, Appl. Surf. Sci. 419 (2017) 522–530.
[23] Wu. Maokun, Xiaolong Yao, Yuan Hao, Hong Dong, Yahui Cheng, Hui Liu, Lu. Feng, Weichao Wang, Kyeongjae Cho, Wei-Hua Wang, Electronic structures, magnetic properties and band alignments of 3d transition metal atoms doped monolayer MoS 2, Phys. Lett. A 382 (2–3) (2018) 111–115.
[24] Federico M. Pesci, Maria S. Sokolikova, Chiara Grotta, Peter C. Sherrell, Francesco Reale, Kanudha Sharda, Na. Ni, Pawel Palczynski, Cecilia Mattevi, MoS2/WS2 heterojunction for photoelectrochemical water oxidation, ACS Catal. 7 (8) (2017) 4990–4998.
[25] Line S. Byskov, Jens K. Nørskov, Bjerne S. Clausen, Henrik Topsøe, Edge termination of MoS2 and CoMos catalyst particles, Catal. Lett. 64 (2–4) (2000) 95–99.
[26] M.V. Bollinger, K.W. Jacobsen, J.K. Nørskov, Atomic and electronic structure of MoS2 nanoparticles, Phys. Rev. B 67 (8) (2003) 085410.
[27] Berit Hinnemann, Poul Georg Moses, Jacob Bonde, Kristina P. Jørgensen, Jane H. Nielsen, Sebastian Horch, Ib Chorkendorff, Jens K. Nørskov, Biomimetic hydrogen evolution: MoS2 nanoparticles as catalyst for hydrogen, Evolution. J. Am. Chem. Soc. 127 (15) (2005) 5308–5309.
[28] Charlie Tsai, Karen Chan, Frank Abild-Pedersen, Jens K. Nørskov, Active edge sites in MoSe2 and WSe2 catalysts for the hydrogen evolution reaction: a density functional study, Phys. Chem. Chem. Phys. 16 (26) (2014) 13156–13164.
[29] Paolo Giannozzi, Stefano Baroni, Nicola Bonini, Matteo Calandra, Roberto Car, Carlo Cavazzoni, Davide Ceresoli, Guido L. Chiarotti, Matteo Cococcioni, Ismaila Dabo, Andrea Dal Corso, Stefano de Gironcoli, Stefano Fabris, Guido Fratesi, Ralph Gebauer, Uwe Gerstmann, Christos Gougoussis, Anton Kokalj, Michele Lazzeri, Layla Martin-Samos, Nicola Marzari, Francesco Mauri, Riccardo Mazzarello, Stefano Paolini, Alfredo Pasquarello, Lorenzo Paulatto, Carlo Sbraccia, Sandro Scandolo, Gabriele Sclauzero, Ari P Seitsonen, Alexander Smogunov, Paolo Umari, Renata M Wentzcovitch, QUANTUM ESPRESSO: a modular and open-source software project for quantum simulations of materials, J. Phys. Condens. Matter 21 (39) (2009) 395502.
[30] P. Giannozzi, O. Andreussi, T. Brumme, O. Bunau, M.. Buongiorno Nardelli, M. Calandra, R. Car, C. Cavazzoni, D. Ceresoli, M. Cococcioni, N. Colonna, I. Carnimeo, A. Dal Corso, S. de Gironcoli, P. Delugas, R.A. DiStasio, A. Ferretti, A. Floris, G. Fratesi, G. Fugallo, R. Gebauer, U. Gerstmann, F. Giustino, T. Gorni, J. Jia, M. Kawamura, H.-Y. Ko, A. Kokalj, E. Küçükbenli, M. Lazzeri, M. Marsili, N. Marzari, F. Mauri, N.L. Nguyen, H.-V. Nguyen, A. Otero-de-la Roza, L. Paulatto, S. Poncé, D. Rocca, R. Sabatini, B. Santra, M. Schlipf, A.P. Seitsonen, A. Smogunov, I. Timrov, T.

Thonhauser, P. Umari, N. Vast, X. Wu, S. Baroni, Advanced capabilities for materials modelling with Quantum ESPRESSO, J. Phys. Condens. Matter 29(46) (2017) 465901.
[31] John P. Perdew, Kieron Burke, Matthias Ernzerhof, Generalized gradient approximation made simple, Phys. Rev. Lett. 77 (18) (1996) 3865–3868.
[32] Stefan Grimme, Jens Antony, Stephan Ehrlich, Helge Krieg, A consistent and accurate ab initio parametrization of density functional dispersion correction (DFT-D) for the 94 elements H-Pu, J. Chem. Phys. 132 (15) (2010) 154104.
[33] Nicola Marzari, David Vanderbilt, Alessandro De Vita, M.C. Payne, Thermal contraction and disordering of the Al(110) surface, Phys. Rev. Lett. 82 (16) (1999) 3296–3299.
[34] David Vanderbilt, Soft self-consistent pseudopotentials in a generalized eigenvalue formalism, Phys. Rev. B 41 (11) (1990) 7892–7895.
[35] Gianluca Prandini, Antimo Marrazzo, Ivano E. Castelli, Nicolas Mounet, Nicola Marzari, Precision and efficiency in solid-state pseudopotential calculations, npj Comput. Mater. 4(1) (2018) 72.
[36] K. Lejaeghere, G. Bihlmayer, T. Bjorkman, P. Blaha, S. Blugel, V. Blum, D. Caliste, I. E. Castelli, S.J. Clark, A. Dal Corso, S. de Gironcoli, T. Deutsch, J.K. Dewhurst, I. Di Marco, C. Draxl, M. Du ak, O. Eriksson, J.A. Flores-Livas, K.F. Garrity, L. Genovese, P. Giannozzi, M. Giantomassi, S. Goedecker, X. Gonze, O. Granas, E.K.U. Gross, A. Gulans, F. Gygi, D.R. Hamann, P.J. Hasnip, N.A.W. Holzwarth, D. Iu an, D.B. Jochym, F. Jollet, D. Jones, G. Kresse, K. Koepernik, E. Kucukbenli, Y.O. Kvashnin, I.L.M. Locht, S. Lubeck, M. Marsman, N. Marzari, U. Nitzsche, L. Nordstrom, T. Ozaki, L. Paulatto, C.J. Pickard, W. Poelmans, M.I.J. Probert, K. Refson, M. Richter, G.-M. Rignanese, S. Saha, M. Scheffler, M. Schlipf, K. Schwarz, S. Sharma, F. Tavazza, P. Thunstrom, A. Tkatchenko, M. Torrent, D. Vanderbilt, M.J. van Setten, V. Van Speybroeck, J.M. Wills, J.R. Yates, G.-X. Zhang, S. Cottenier, Reproducibility in density functional theory calculations of solids, Science 351(6280) (2016) aad3000–aad3000.
[37] Jun Cheng, Xiandong Liu, John A. Kattirtzi, Joost VandeVondele, Michiel Sprik, Aligning electronic and protonic energy levels of proton-coupled electron transfer in water oxidation on aqueous TiO 2, Angew. Chem. Int. Ed. 53 (45) (2014) 12046–12050.
[38] J.K. Norskov, J. Rossmeisl, A. Logadottir, L. Lindqvist, J.R. Kitchin, T. Bligaard, H. Jónsson, Origin of the overpotential for oxygen reduction at a fuel-cell cathode, J. Phys. Chem. B 108 (46) (2004) 17886–17892.